Original Paper

Indoor and Built Environment

Indoor and Built Environment
2017, Vol. 26(6) 771–784

DOI: 10.1177/1420326X16638912
journals.sagepub.com/home/ibe
SAGE

Thermographic and mobile indoor mapping for the computation of energy losses in buildings

L. López-Fernández[1], S. Lagüela[1,2], D. González-Aguilera[1] and H. Lorenzo[2]

Abstract
A mobile indoor mapping system combined with infrared thermography was used for the acquisition of data needed for the quantification of heat loss through a building envelope by conduction; that is, temperature values and building geometry. The methodology presented orthothermograms to provide measurement of heat loss and thermographic images with geometric information. This way, not only the energy loss through the building envelope is provided, but also thermographic information regarding the existence of thermal pathologies, their location and their impact on the building can also be evaluated.

Keywords
Infrared thermography, Thermal pathology, Point cloud, Mosaic, Heat losses, Building envelope, Indoor mapping

Accepted: 23 February 2016

Introduction

The use of infrared thermography as a widely tested technique for building inspection and location of pathologies such as air leakage and moisture[1–3] allows the performance of quality, quick, effective and non-destructive 'in-situ' inspections without direct contact with the object under study. This qualitative measurement technique has been used for detecting and localizing thermal and physical pathologies by some authors to perform in-situ studies, mainly in historical buildings or cultural heritage elements.[4,5] On the other hand, quantitative approaches have been performed mainly in laboratories with limited sample size.[6,7] In those cases where these quantitative thermography studies were performed in-situ,[8,9] temperature values were accurately measured in order to be used for the computation of the real thermophysical properties (thermal conductivity) of the building envelope, but their spatial distribution has not been considered. If the constituent materials are taken into account, infrared thermography should also be used for the determination of thermophysical properties such as diffusivity and thermal transmittance.[10,11]

Regarding geometry, the complex geometry of building indoors and the common presence of furniture and other elements, the use of static terrestrial laser scanning systems would entail a time-consuming data acquisition, since a high number of measuring positions would be needed to provide a full coverage of the scene. In this sense, the use of a mobile 'indoor mapping' laser scanning system is considered as the ideal technique for data recording, ensuring enough quality and speed.

In order to fill these gaps and obtain a thermographic-metric result, an approach combining both qualitative and quantitative measurement techniques was applied in our present study. Qualitative thermography was used for the automatic classification of the

[1]Department of Cartographic and Land Engineering, University of Salamanca, Hornos Caleros, Ávila, Spain
[2]Applied Geotechnologies Research Group, University of Vigo, Vigo, Spain

Corresponding author:
L. López-Fernández, Department of Cartographic and Land Engineering, University of Salamanca, Hornos Caleros, Ávila, Spain.
Email: luisloez89@usal.es

façade elements, while quantitative techniques were used for the measurement of temperatures of the wall and the pathologies, and the subsequent computation of heat loss. In addition, the spatial distribution of the pathologies was accurately assessed through the combination of thermographic images with the point cloud acquired with an indoor mapping system. The registration of the thermographic images with the point clouds was performed through the identification of homologous points between the thermograms and the point clouds allowing the computation of the spatial resection parameters.[12] What is more, the computation of the heat loss by conduction through the building envelope was automated, based on the temperatures measured with a thermographic camera and the geometry measured by an indoor mapping system through the automated generation of orthothermograms. In this way, thermography was used to represent the state of the wall, and to quantify the energy loss through it.[13–15] In addition, the generated orthothermograms can be used for the determination of energy losses in buildings.

Materials and methods

Equipment

Data acquisition was performed with two different systems. The geometric information was acquired with an indoor mapping system to generate point clouds of building interiors simultaneously to the displacement of the platform. Temperatures were measured with a thermographic camera, acquiring thermographic images of every wall. Both systems were used separately in this study.

Indoor mapping unit. The indoor mapping unit (Figure 1) was equipped with positioning systems and geomatics sensors for the generation of 3D point clouds of the buildings inspected.

In particular, the positioning systems used, were an inertial measurement unit (IMU) 'spatial' from 'advanced navigation' (Table 1) and two dual channel 'Kübler' odometers able to register a total of 128 counts per channel. These sensors were used to perform the computation of the trajectory followed by the mapping unit from the measurements of the rotation in the three axes and the longitudinal displacement in the plane.[16]

Regarding the geomatics sensors, the indoor mapping unit was equipped with a time of flight laser scanner, 'Hokuyo UTM-30LX', with a measuring range of 30 m and an angular resolution of 0.25°, with 30 mm precision.[17]

The laser sensor has a measurement frequency of 25 ms^{-1}. During this time the laser emits rays sweeping an arc of 270°. Given this fact, the sensor was positioned in the indoor mapping system in a horizontal position, measuring profiles perpendicular to the trajectory, and the coordinates measured for each point were (y, z). The 90° angle where no measurements were performed was oriented towards the floor, in such a way that no information would be missed from the walls and the ceiling of the building inspected, as shown in Figure 1.

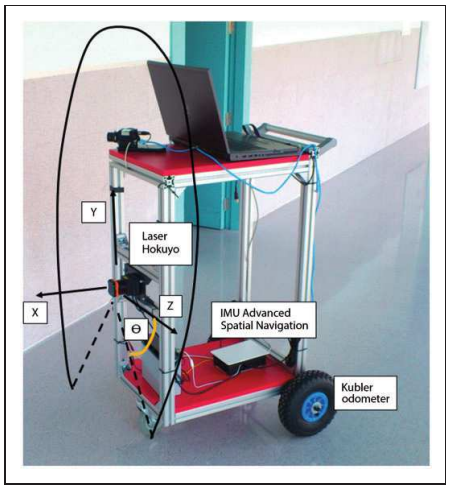

Figure 1. Diagram of the indoor mapping unit, the position of the different sensors and the axes assigned to the different components of movement.

Measurements of the laser and the positioning sensors were simultaneously acquired. Each 2D profile (y, z) from the laser has a time stamp for its association with the position data of the mobile unit during acquisition. Because of this time stamp, the position of each laser profile in the trajectory was used for the generation of a complete 3D point cloud of the building inspected[18] but without GPS data. The position was assumed as the x coordinate, therefore each point would be assigned its (x, y, z) coordinates.

Thermographic camera. Thermographic data acquisition was performed with a camera NEC TH9260 (Figure 2, left), measuring temperatures in a range from −20°C to 60°C, with a thermal resolution of 0.006°C at 30°C (30 Hz). The sensor was an Uncooled Focal Plane Array (UFPA), 640 × 480 size, capturing radiation between 7 and 14 μm wavelength. The instant field of view (IFOV) of the camera was 0.6 mrad, and its field of view with the current lens of 20 mm focal length was 21.7° (Horizontal – H) and 16.4° (Vertical – V). The IFOV (typically described in milliradians)

Table 1. 'Spatial' IMU specifications.

Sensor	Accelerometers	Gyroscopes	Magnetometers	Pressure
Range (dynamic)	2 g	250°/s	2 G	10 to 120 KPa
	4 g	500°/s	4 G	
	16 g	200°/s	8 G	
Bias Instability	20 μg	3°/h	–	10 Pa
Initial bias	< 5 mg	< 0.2°/s	–	< 100 Pa
Initial scaling error	< 0.06%	< 0.04%	< 0.07%	–
Scale factor stability	< 0.06%	< 0.05%	< 0.09%	–
Non-linearity	< 0.06%	< 0.05%	< 0.08%	–
Cross-axis Alignment Error	< 0.05 °	< 0.05 °	< 0.05 °	–
Noise density	150 μg/√Hz	0.005°/s/√Hz	210 μG/√Hz	0.56 Pa/√Hz
Bandwidth	400 Hz	400 Hz	110 Hz	50 Hz

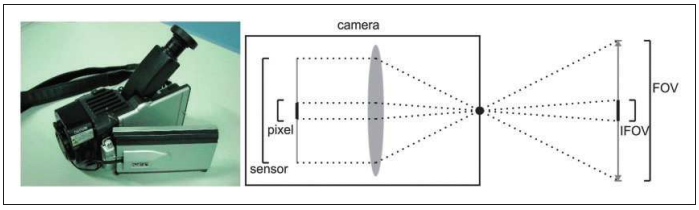

Figure 2. Thermographic camera used in this study (left). FOV and IFOV diagram of the thermographic camera (right).

corresponds to the two dimensional (H and V) angular area which was viewed by a single pixel of the detector through the optics of the camera. This defines the spatial resolution, or the size of the smallest object that can be viewed or resolved at a specific distance from the camera. The FOV (typically described in horizontal degrees by vertical degrees) can be defined as the largest area that an imaging sensor can capture at a set distance (Figure 2, right).

The main advantage of this camera for its use in the presented methodology is the availability of its geometric calibration, so that its inner orientation parameters are known, such as the principal point, sensor size and lens distortion coefficients. This calibration was previously performed using a specially designed calibration field.[19]

In addition to the thermographic camera, the acquisition of thermal data was complemented with a contact thermometer TESTO 720 (Table 2), which was used for the measurement of the inner and outer ambient temperature to perform the energy consumption analysis, and the temperature of the walls in certain points was measured to perform an emissivity correction of each thermography. This way, all data needed for the energy analysis, and for the emissivity correction of the values which were measured in the thermographic images, were recorded.

Table 2. Testo 720 specifications.

Parameter	Value
Range	−50°C to 150°C
Accuracy	±0.2°C (−25°C to +40°C)
	±0.3°C (+40.1°C to +80°C)
	±0.4°C (+80.1°C to +125°C)
	±0.5°C (<25°C and >125°C)
Resolution	0.1°C

There are three different sources of infrared (IR) radiation that can be captured by the thermographic camera if we assume that the object under study is opaque, implying that the transmission of IR radiation is null. These are the emission from the object under study; the reflected radiation from the surroundings (both attenuated by the atmospheric transmission) and the emission from the atmosphere[20] (Figure 3).

The emissivity correction was based on Stefan-Boltzmann's law (1), assuming that a real body with a surface temperature measured by a thermometer can be considered as a real body, whereas they can be considered as black bodies when temperature values are measured with a thermographic camera (with no emissivity

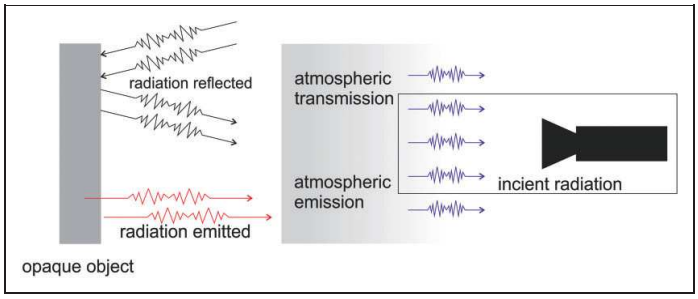

Figure 3. Components of incident IR radiation acquired by the thermographic camera.

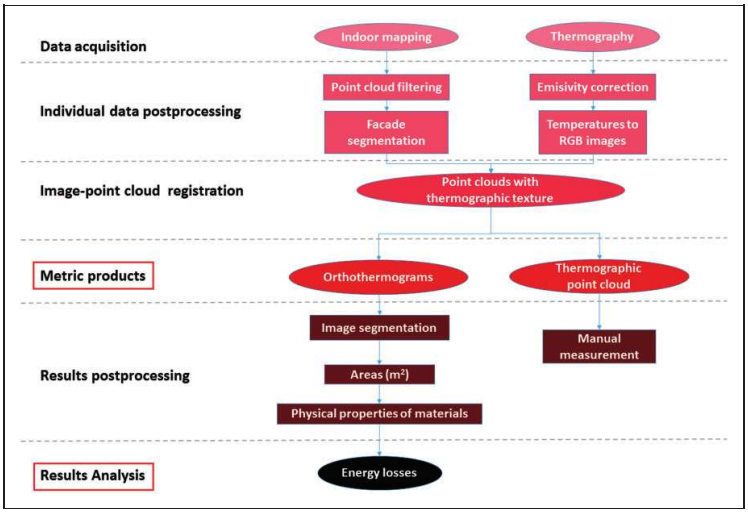

Figure 4. Workflow representing the methodology developed for the automatic quantification of energy losses and pathologies assessment in buildings using data acquired with a mobile indoor mapping unit and a thermographic camera.

correction introduced in the camera parameters). This way, emissivity can be defined by equation (1) as

$$\varepsilon_{rb} = \frac{T_{rb}^4}{T_{bb}^4} \quad (1)$$

where 'T_{bb}' is the temperature measured with the thermographic camera, and 'T_{rb}' is the temperature measured by the contact thermometer.

The correction of the atmospheric effect was directly performed by the thermographic camera through the configuration of the ambient parameters (temperature and humidity) and the camera–object distance.

Methodology

The proposed methodology (Figure 4) consists of three steps, and these are defined as follows:

- Data acquisition and pre-processing.
- Data processing and registration.
- Result interpretation

Data acquisition. This procedure involves the acquisition of both thermographic images and 3D point clouds.

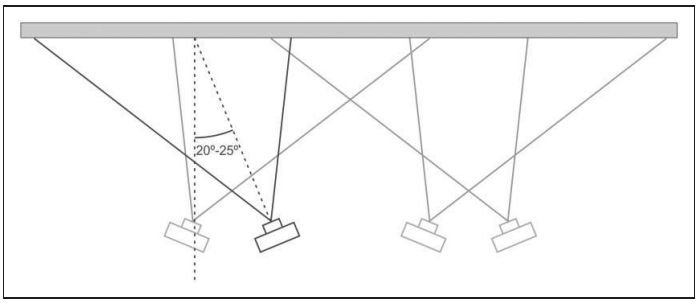

Figure 5. Overlapping between images and angle of incidence between the camera optical axis and the evaluated surface.

Thermographic images: Given the influence of the external parameters in the measurements performed with thermographic cameras, the establishment of a protocol for data acquisition was required for the minimization of these effects and the acquisition of valid products for their processing and analysis.

The *first rule* in the protocol is the existence of an approximate 10°C difference between the indoor-to-outdoor average temperature difference of the building (standard temperature difference considered for these studies) for maximizing the detection of the existing pathologies, like insulation deficiencies or moisture.[21] For example, the type of construction and location of the insulation layer within the building envelope could influence the temperature conditions under which pathologies may be detected. A minimum indoor-to-outdoor average temperature difference could mean inaccuracies in the pathologies detection, and this process could even become unapproachable. Although precipitation would be a significant issue for external surveys and less relevant to the type of internal survey reported in this study, prior building inspection is recommended to ensure no precipitation occurs for at least 24 h.

The *second rule* is the acquisition of thermographic images with an angle of incidence of 20° or 25° between the normal of the wall under study and the optical axis of the camera (Figure 5), therefore, avoiding the influence of the infrared radiation that would be emitted by the operator and reflected from other surfaces on the recorded thermal pattern.

The *third rule* is the adjustment of the ambient parameters in the camera; that is, distance camera–object, ambient temperature and humidity, prior data acquisition.

The *fourth rule* is the preparation of the survey in order to achieve an approximate steady-state heat transfer through the building envelope conditions. In particular, this would require a historical study of the temperatures of the building location in order to perform the survey in a time slot where the variation of the exterior temperature could be minimized. The survey should be conducted in winter as recommended, with overcast skies and at night, some hours after sunset if possible, in order to minimize the solar gain effect over the façades.

Given the limited field of view of the thermographic camera used, several acquisitions were required for the inspection of the total surface under study. This would require the maintenance of a minimum 10% overlap between consecutive images for the posterior generation of one product to represent completely the surface under study.

Point clouds: Planning data acquisition with the indoor mapping unit was required for the optimization of the quality of the data acquired.

The main error source of these devices comes from the Inertial Measurement Unit. In order to minimize the drift, the trajectory should avoid sharp turns that imply unnecessary drift accumulations, as well as avoiding every obstacle that could block or modify the trajectory of the indoor mapping unit. The displacement over sliding surfaces should be avoided, in order to minimize the risk of having inconsistent readings in the odometers that imply great deviations in the posterior computation of the trajectory, as well as incoherent data between these sensors and the inertial unit.

The IMU could be affected by external electromagnetic sources, such as metallic material, wiring, magnets and electrical transformers, to produce unacceptable variations in the measurement. For this reason, the presence of these objects should be considered and avoided if possible.

Finally, the measurement range of the laser scanner in the indoor mapping unit was taken into account for the definition of the trajectory with the aim of guaranteeing a continuous data acquisition for these scenes under study.

Image-point cloud registration. The transmission of the thermographic texture to the point

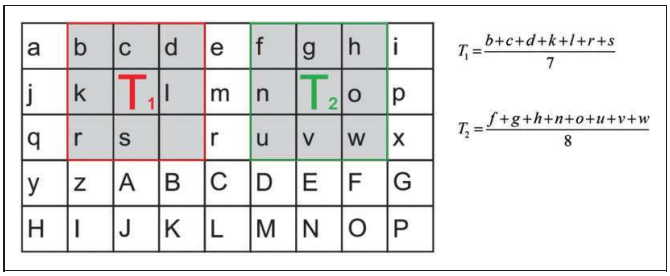

Figure 6. Convolution mask for solving the resampling of those pixels without thermographic texture. The different examples show that the mask ignores no-texture pixels for the computation.

cloud obtained with the indoor mapping unit was developed through the computation of the spatial resection[12] of the thermographic images using the laser scanning point cloud as reference and the identification of homologous entities (interest points) between each image and the point cloud by a human operator. The spatial resection would make use of image coordinates and their homologous object coordinates to determine the position and orientation of the camera.[22]

Once the exterior orientation of each thermography was calculated, the thermographic texture was transmitted to the point cloud. The result obtained was a thermographic point cloud where each point would have a temperature value associated and represented by the RGB conversion to the defined colour map.

The next step involved the orthogonal projection of each wall of the scene to their corresponding parallel planes, in a procedure where an image called orthothermogram was generated. Orthothermograms are images with geometric scale and no distortion, in such way that the measurement of a distance on the image, multiplied by the scale, would result in the measurement in the reality. Given that the procedure of projecting the thermographic point clouds into a plane would result in an image with occlusions or areas with missing information, an adaptive resampling algorithm was applied in order to cover the existing gaps between pixels. This algorithm would require the implementation of a convolution mask size 3×3 to work on the pixels that was lacking in thermographic texture by evaluating the surrounding pixels and using only those pixels with thermographic texture for the computation of the mean temperature (Figure 6).

Orthothermogram segmentation. The thermographic-metric results generated permit the performance of accurate analysis of the energy consumption of the building under study. The point cloud with thermographic texture allows analysis of the 3D model of the building directly and to extract accurate information of the elements of interest. However, the energy study was focused on the analysis of the orthothermograms.

According to the Spanish Technical Code for Buildings (Código Técnico de Edificación, CTE),[23] the computation of heat losses through a building envelope requires the location of the areas corresponding to the walls, openings (windows) and thermal bridges reflected in the orthothermograms. The different values of thermal emissivity of the principal construction elements (walls, windows and thermal bridges) allow the segmentation process through the study of the reflected temperatures and the thermal gradients.

The segmentation of the zones of interest was performed in two steps. (i) First, identify the critical points on the envelope (pathologies, differentiating between moisture and thermal bridges) and (ii) Second, recognize the openings. For this purpose, each orthothermogram was divided into two different orthothermograms in grey scale: one for the high-temperature areas, and another for the low-temperature areas, using as cutting point the mean value of the temperatures appearing in the image. The result to this segmentation was an orthothermogram with the openings (high-temperature), and an orthothermogram with the existing pathologies (low-temperature): from thermal bridges to damp areas.

The next step consisted the binarization of each image, for the identification of the areas of interest and the elimination of wrongly classified surfaces. This process required the user interaction for the choice of a binarization coefficient that guarantees the expected results. The resultant Boolean image was subjected to a supervised selection of areas of interest allowing the elimination of the noise introduced in the resampling step (pixels without neighbours), as well as the elimination of false positive clusters that did not correspond to elements of interest (these being pathologies and openings).

Once the Boolean image was generated with the zones of interest, the area of each zone was computed thanks to the knowledge of the GSD (Ground Sample

Distance)[24] of the orthothermogram. In particular, the areas corresponding to openings and critical points of the façade were obtained through the multiplication of the number of pixels overpassing the process of feature extraction by the GSD of the orthothermogram. Areas corresponding to walls were obtained through the difference between the total area of the façade and the openings' area.

At this point, the characteristic elements were accurately measured with minimum user interaction.

Heat loss computation. The computation of the energy loss of a building façade entails the study of the thickness, area and thermal properties of the materials used in the building construction. The thermal properties of the materials were determined by their thermal transmittance, U (W/m^{2}K), which represents the rate of heat transfer through 1 m^2 of a structure divided by the temperature difference across the structure. The study was based on an approximate steady-state heat transfer, as an acceptable approximation for conditioned buildings in climates with small solar gains and small outdoor temperature oscillation amplitude as compared with the indoor-to-outdoor average temperature difference. For the sake of simplification, U-values were considered as constant with temperature[25] omitting the effect of solar gain on heat transmission through the fabric, minimized by the implementation of the survey under guidelines described above. This parameter is defined by equation (2)

$$U = {}^{1}/_{R_t} \tag{2}$$

where 'U' represents the thermal transmittance and 'R_t' is the total thermal resistance of the construction element (m^{2}K/W).

Given that the wall of the building under study was composed of several layers of different materials, the total thermal resistance was calculated as the sum of the thermal resistance of each layer and the superficial thermal resistances of the inner and outer air.

The effect of the thermal bridges was considered through the computation of the heat transfer by transmission coefficient of the surface 'H_T', calculated by equation (3).

$$H_T = \sum_i A_i U_i + \sum_i l_k \psi_k \tag{3}$$

where 'U' is the thermal transmittance of the wall analysed (W/m^{2}K), 'A' is the area of the wall under study (m^2), 'ψ_k' is the lineal thermal transmittance of the thermal bridge (W/mK) and 'l' is the length of the thermal bridge (m).

After the computation of the heat transfer by transmission coefficient of the wall, the computation of the energy loss can be determined. The heat loss by conduction through the envelope of a building due to the thermophysical properties of the constructive materials can be determined by equation (4).

$$Q = H_T \cdot (T_{int} - T_{ext}) \tag{4}$$

where 'Q' is the heat loss through the wall analysed (W), 'H_T' is the heat transfer by transmission coefficient (W/K) and 'T_{int}' and 'T_{ext}' are the interior and exterior temperatures, respectively (K).

The thermal transmittance of the openings was computed using the knowledge of the materials composing these elements and their corresponding thermal transmittances, as well as the percentage of opening occupied per material.

From these data and following the standard established by the CTE, the total thermal transmittance of the openings, U_H, was computed with equation (5).

$$U_H = (1 - FM) \cdot U_{H,v} + FM \cdot U_{H,m} \tag{5}$$

where 'U_H' is the total thermal transmittance of the opening, '$U_{H,v}$' is the thermal transmittance of the semi-transparent surface, and '$U_{H,m}$' is the thermal transmittance of the window frame; all of them in W/m^{2}K. Finally, 'FM' is the opening percentage occupied by the frame (%).

In this case, the evaluation of the effect of any thermal bridge is not necessary, as it is possible to calculate directly the heat loss through the openings using the equation (6)

$$Q_H = U_H \cdot A \cdot (T_{int} - T_{ext}) \tag{6}$$

where 'Q_H' is the heat loss through the opening analysed (W).

The heat losses were computed following the protocol described in the CTE which would reflect the energy loss assuming an 'ideal' condition of the envelope. However, reality shows the presence of thermal pathologies in the building envelopes, directly affecting the energy consumption.

As a result, the additional heat loss through the building envelope on the critical surfaces was computed using equations (3) and (4), but considering only the area of those surfaces with pathologies without the thermal bridging effect, and the temperature difference between the surface with pathologies and the undamaged wall. For the sake of simplification, the increase of heat loss through the critical surfaces can be calculated using equation (7):

$$Q_c = U \cdot A_c \cdot (T_m - T_c) \tag{7}$$

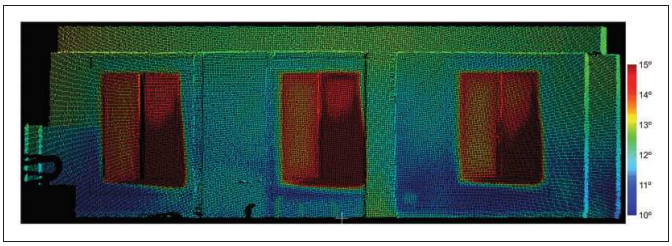

Figure 7. Point cloud with thermographic texture (south façade).

where Q_c is the additional energy loss through the critical surfaces (W) in addition to the heat loss as a function of the building composition; U is the total thermal transmittance of the wall (W/m^{2}K) and A_c is the total critical area (m^2). T_m is the mean temperature of the wall in good conditions (K), and T_c is the mean temperature of the critical surface in the wall (K).

Experimental results

Case study

The proposed methodology was validated in a building chosen by its architectural importance, in the town of Baiona (Northwest Spain). Currently, the building has been dedicated to music education so, the study must be performed during the day in order to measure the energy demand in the time slot when the infrastructure was being used and the HVAC (Heating, Ventilation and Air Conditioning) instruments should be working to maintain the adequate thermal comfort. The survey was performed on March 2013 under partly cloudy sky conditions in order to minimize the outside temperature variations during the survey process and the effect of direct solar irradiation incidence. After the historical temperature analysis, the optimum time slot to perform the survey was defined between 11:00 and 13:00 hours. The study was undertaken prior to the refurbishment of the building. The conservation condition of the inner face of the façades was evaluated and the existence of any thermal pathology was determined and detected to minimize any would be increase in energy consumption for heating the building.

Thus, the proposed methodology was applied to each façade of the building under study. Both the structure of each façade and the thermophysical properties of the thermal bridges was obtained from the technical documentation included in the building construction project. Walls of the building were composed of homogeneous layers of granite and bricks, also with a non-ventilated cavity wall and a thermal insulation of mineral wool. The openings are windows with aluminum frames with single-pane glazing.

Atmospheric conditions during data acquisition were 6°C exterior air temperature, while the interior air temperature was 13°C measured with the contact thermometer.

Data combination

The first step for the combination of the dataset was the computation of the orientation of each thermographic image regarding the point cloud of the building. For this purpose, the maximum number of significant features in each thermographic image was identified by a human operator, consequently minimizing the error in the computation of the external orientation parameters. Once the orientation parameters were computed per thermographic image, and the thermographic texture was transferred to the point cloud, the product was a point cloud with thermographic texture (Figure 7).

Metric thermographic images

The thermographic point cloud was subjected to the generation of an orthothermogram per wall (Figure 8), and a re-sampling process for the minimization of areas with no information.

Orthothermogram segmentation

The orthothermogram of each wall was subjected to an operation of automatic segmentation of the zones of interest so that they can be used for the quantification of the heat loss through the wall. This process requires a classification of the pixels into two groups: one for highest temperatures, where openings are; another for lowest temperatures, where the critical surfaces of the façade can be identified (Figure 9). Consequently, two orthothermograms were obtained: one for the openings, one for the pathologies. In this case study, consisting of a room with closed shutters at the moment of

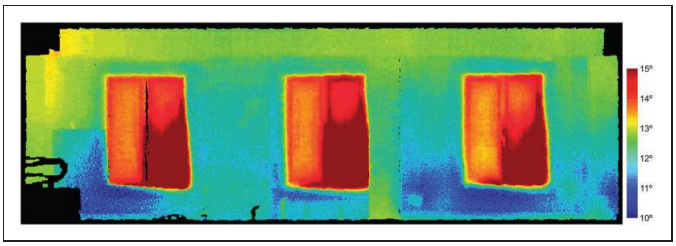

Figure 8. South façade: Orthothermogram after resampling with a GSD of 1 cm.

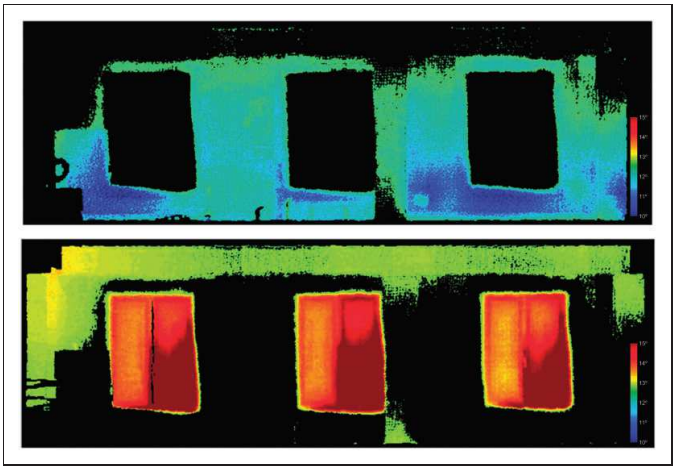

Figure 9. South façade: (top) Low-temperature group. (bottom) High-temperature group.

the inspection, the Sun was radiating on the windows, leading to their overheating. This is the reason for the presence of windows in the high-temperature group. What is more, the main pathology of the building was moisture, presenting low temperature due to the cooling of the surface caused by evaporation. Moisture was easily differentiated in the thermal images by its geometry, location and temperature difference with the undamaged wall. In addition, some zones with pathologies related with air leakage were characterized by larger temperature variations than those produced by moisture and being located in junctions between different elements of the façade.

Group images were segmented in the different zones of interest corresponding to the windows and critical surfaces, resulting in a binary image for each element.

Finally, a visual inspection by a human operator was required with the aim of eliminating the noise introduced in the orthothermograms during the re-sampling step, as well as to overcome the binarization process within the zones that do not represent any element of interest (Figure 10).

Energy analysis

Walls. The segmented orthothermograms provide information of the area of the different elements of interest. Consequently, only the thermophysical parameters of the materials obtained directly from the syllabus of construction solution of the CTE[26] and their thickness in the wall (Table 3), were needed for the determination of the energy requirements of each façade, following the indications of the CTE and the methodology presented in section 'Heat loss computation'.

Each wall of the scene under study was composed by one layer of granite with 0.2 m of thickness, 0.05 m of

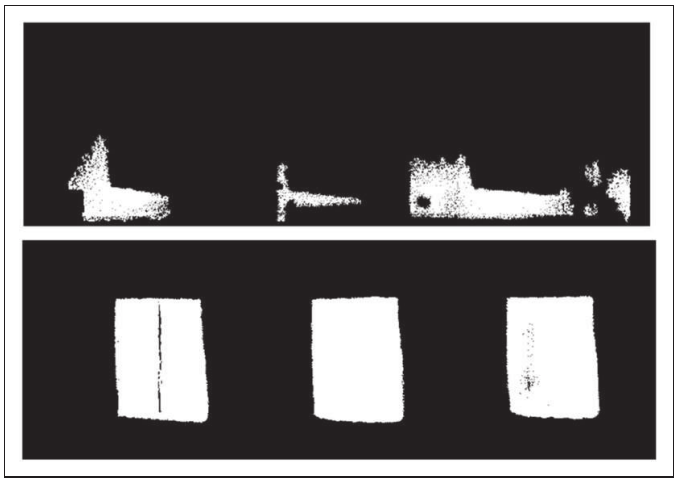

Figure 10. South façade: (top) Final binary image with critical surfaces (pathologies). (bottom) Final binary image with windows.

Table 3. Thermal resistance, thermal conductivity and thickness of the elements involved in the calculation of the thermal transmittance of the wall.

Material	Thickness (m)	Thermal conductivity (W/m·K)	Thermal resistance (m^2K/W)
Granite	0.2	2.8	0.071
Bricks	0.045	0.214	0.210
Non-ventilated cavity wall	0.05	–	0.180
Thermal insulation (Mineral wool)	0.02	0.031	0.645
Plastering	0.015	0.57	0.026
Inner air 'R_{SI}'	n/a	n/a	0.130
Outer air 'R_{SE}'	n/a	n/a	0.040
Total thermal resistance of the wall			1.302

Source: CTE.[26] *Openings*. n/a: not applicable

non-ventilated cavity wall with 0.02 m of thermal insulation made of mineral wool and 0.045 m of bricks finished with 0.015 m of plastering (Figure 11). The thermal resistance for this composition was 1.302 m^2K/W giving a total thermal transmittance value 'U' of 0.768 W/m^2K.

All window openings (Table 4) were composed with a simple insulated glass (4–6–4 mm) within an aluminum frame covering 20% of the opening.

Thermal bridges. The thermal bridging effect produced by junctions between walls with the floor, windows and other walls, as well as in the pillars where the uniformity of the façade is broken was evaluated by the study. The linear thermal transmittances of the thermal bridges were obtained from the catalog included in the building construction project. The length of the thermal bridges was obtained directly from the geometric information in the orthothermograms (Table 5).

The effect of the thermal bridges was applied to the calculation of the thermal transmittance based on the area of the walls to provide a heat transfer with a transmission coefficient 'H_T' of 135.052 W/K.

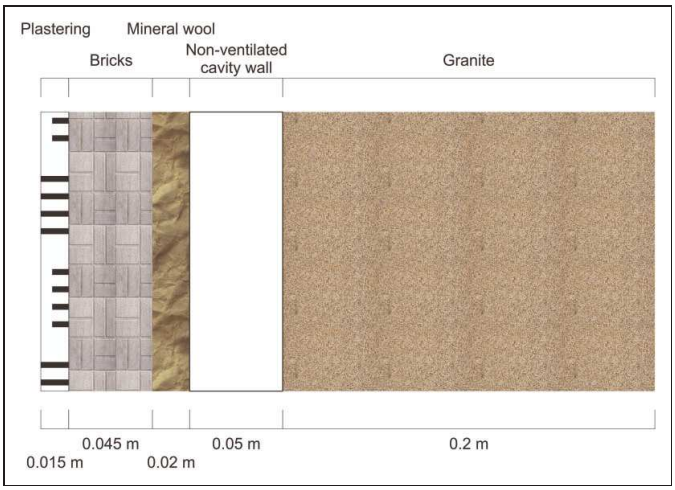

Figure 11. Composition diagram of the wall.

Table 4. Thermal transmittance and percentage per material in the openings.

Material	Thermal transmittance (W/m^2K)	% in the opening
Glass (4 + 6 + 4) mm	3.6	80
Aluminium frame	7.2	20

Source: CTE.[26]

Table 5. Linear thermal transmittance and length of the thermal bridges.

Thermal bridge	Linear thermal transmittance (W/mK)	Total length of the thermal bridge (m)
Junction between walls	0.09	13
Junction between wall and floor	0.96	44.4
Junction between wall and window	0.25	50
Junction between wall and pillar	0.27	41.6

Final results

The application of the proposed methodology had generated two different output results:

- Thermographic point cloud and orthothermograms: 3D point cloud with thermographic texture, allowing the visual inspection of the scene under study, and the preliminary geometric analysis directly measuring the point cloud (Figure 12). The complementary result is the orthothermogram of each façade, used for the automatic determination of the energy requirements of the building. Orthothermograms can also be imported in CAD software for further analysis.
- Heat loss computation per façade as a function of the temperature of the construction element and the area of the wall. Software has been developed for the generation of a file with data of the area occupied per element of interest. This was determined after a semi-automatic segmentation process and the computation of the total thermal transmittance. The knowledge of the specific heat loss through each construction element would allow the identification of the most critical elements towards the refurbishment of the building, and the effect of refurbishment in the total energy consumption of the building under study (Table 6).

Discussion

The first decision to be taken for the development of the present procedure is the configuration of the data acquisition system. In this case, the integration of the

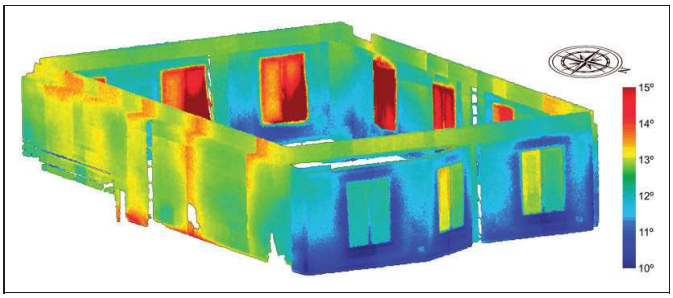

Figure 12. External view of the point cloud with thermographic texture. Holes created by obstacles as well as the side of columns that have not been caught due to the path followed by the indoor mapping unit, were also captured. However, these areas should also be taken into account for the energy analysis.

Table 6. Results obtained after the application of the algorithm developed in this study to the building under study.

	Façade				
	North	South	East	West	Total
Total area (m^2)	24.959	23.018	35.149	34.435	117.561
Wall area (m^2)	19.958	17.331	29.024	34.435	100.748
Window area (m^2)	5.001	5.687	6.125	0	16.813
Pathologies area (m^2)	4.183	0.940	1.599	0	6.722
Total thermal transmittance, wall ($W/(m^2\ K)$)			1.302		
Heat transfer by transmission coefficient of the wall (W/K)			135.052		
Total thermal transmittance, opening ($W/m^2\ K$)			4.320		
Heat loss through the wall in good condition (W)					945.364
Heat loss through the critical surfaces (W)	35.503	9.035	15.378	0	59.916
Total heat loss in the wall (W)					1005.280
Total heat loss in the openings (W)	151.233	171.972	185.217	0	508.422
Total heat loss through the façade (walls + openings) (W)					1513.702

camera in the indoor mapping system would remove the flexibility in data acquisition, both spatial and temporally.[27] Regarding spatial flexibility, the angle for image acquisition would be limited by the position of the camera in the indoor mapping system and the displacement direction, preventing the acquisition of images from other angles of interest. This fact is especially critical for the upper and lower parts of the walls, not visible from the height of the indoor mapping system (Figure 13).

Furthermore, the performance of an optimal thermographic inspection would imply the modification of the trajectory of the indoor mapping system, distorting the geometric data acquisition.

Regarding temporal flexibility, the possibility of completing the thermographic inspection at night separately from the laser scanning to reduce the influence of solar gains would be lost.

With respect to the error caused in temperature measurement and, consequently, in the computation of the energy loss, the accuracy of the thermographic camera and the contact thermometer were 2°C and 0.5°C, respectively. The uncertainty associated to each emissivity correction value can be calculated through the simplified uncertainty propagation method for a non-linear combination of independent variables. Through this uncertainty evaluation method for the least favourable case within the range of measured temperature values, the uncertainty associated to each emissivity correction value was lower than 0.6°C.

Considering that, for this study, only the relative values along the surfaces were evaluated in order to

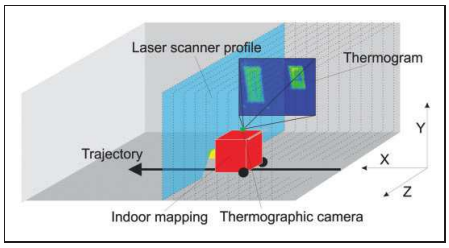

Figure 13. Limitations of using a thermographic camera mounted onboard the indoor mapping system. Due to the limited field of view of the thermographic camera, walls are not fully covered if images are acquired from the indoor mapping system.

segment the façades in their different components, the correction of the reflected temperatures was not necessary, assuming that their effect would be uniform over the whole surface and would not affect the relative difference between temperatures.

The use of infrared thermography would allow the estimation of these energy losses due to the accurate identification of the critical points and the thermal differences existing between these and non-critical surfaces. A similar analysis was performed by Asdrubali et al.[28] for the characterization of thermal bridges, and by González-Aguilera[29] through the classification of the building envelope using isotherms.

Conclusions

This article presents a methodology for the generation of thermographic point clouds and orthothermograms, as well as the computation of heat losses through walls based on the semi-automatic integration of thermographic images and indoor point clouds which were applied to indoor building scenes. The results obtained have provided complete thermographic and metric information of the different elements, to enable a better detection, spatial location and interpretation of thermal pathologies than a single thermal image. The geometric information embedded on the orthothermograms enables the measurement of areas and distances for the quantification of energy losses and thus allows the determination of any increase in the energy consumption that could be caused by the existence of pathologies.

The methodology could provide a suitable routine method to accurately evaluate the state of buildings prior to refurbishment in order to assess the need to invest in the partial or total refurbishment of the façade and calculate an approximation of the refurbishment effect on the heat loss transmission resulting in energy savings.

The main problem of the presented methodology is the complexity of the automation of the detection of thermal pathologies mainly due to the high number of factors to consider in the thermal imaging interpretation, such as environmental conditions, solar impact, surface state of the element under study and emissivity. This problem can be solved by specifying an appropriate temperature interval for the representation of temperature differences for the object analysed, so that the detection of areas affected by pathologies is maximized, allowing the performance of appropriate binarization of the orthothermograms.

Authors' contribution

All authors contributed equally in the preparation of this manuscript. SLL performed the data acquisition, LLF developed data processing and analysis; data interpretation was made by LLF, SLL and DGA.

Declaration of conflicting interests

The author(s) declared no potential conflicts of interest with respect to the research, authorship, and/or publication of this article.

Funding

The author(s) disclosed receipt of the following financial support for the research, authorship, and/or publication of this article: The authors would like to thank the Ministerio de Educación. Cultura y Deporte (Gobierno de España) for the financial support given through human resources programs (FPDI-2013-17516). Also, they thank the support given by the Ministerio de Economía y Competitividad through projects ENE2013-48015-C3-1-R.

References

1. Grinzato E, Vavilov V and Kauppinen T. Quantitative infrared thermography in buildings. *Energ Build* 1998; 29: 1–9.
2. Rosina E and Spodek J. Using infrared thermography to detect moisture in historic masonry: a case study in Indiana. *APT Bull* 2003; 34: 11–16.
3. Li H, Gong G, Xu C, Su H, Cao Z, Zhou M and Yu CWF. Thermal and humid environment and moisture condensation characteristics of cold surfaces. *Ind Built Environ* 2014; 23: 474–484.
4. Avdelidis N and Moropoulou A. Applications of infrared thermography for the investigation of historic structures. *J Cult Herit* 2004; 5: 119–127.
5. Tavukcuoglu A, Duzgunes A, Demirci S and Caner-Saltık EN. The assessment of a roof drainage system for an historical building. *Building Environ* 2007; 42: 2699–2709.
6. Bison P and Grinzato E. IR thermography applied to the assessment of thermal conductivity of building materials. SPIE Defense, Security, and Sensing. *Int Soc Opt Photon* 2010; 7661: 76610G–G-9.
7. Barreira E and de Freitas VP. Evaluation of building materials using infrared thermography. *Constr Build Mater* 2007; 21: 218–224.

8. Lagüela S, Díaz-Vilariño L, Armesto J and Arias P. Non-destructive approach for the generation and thermal characterization of an as-built BIM. *Constr Build Mater* 2014; 51: 55–61.
9. Fokaides PA and Kalogirou SA. Application of infrared thermography for the determination of the overall heat transfer coefficient (U-Value) in building envelopes. *Appl Energ* 2011; 88: 4358–4365.
10. Mercuri F, Zammit U, Orazi N, Paoloni S, Marinelli M and Scudieri F. Active infrared thermography applied to the investigation of art and historic artefacts. *J Therm Anal Calorimetr* 2011; 104: 475–485.
11. Vavilov V, Kauppinen T and Grinzato E. Thermal characterization of defects in building envelopes using long square pulse and slow thermal wave techniques. *J Res Nondestr Eval* 1997; 9: 181–200.
12. Kraus K. Advanced methods and applications. Vol. 2. *Fundamentals and Estándar processes. Vol.* 1. Institute for Photogrammetry Vienna University of Technology, Ferd Dummler Verlag Bonn. Bonn, Germany, 1993..
13. Lagüela S, Díaz-Vilariño L, Martínez J and Armesto J. Automatic thermographic and RGB texture of as-built BIM for energy rehabilitation purposes. *Automat Constr* 2013; 31: 230–240.
14. Hoegner L and Stilla U. Automatic generation of façade textures from terrestrial thermal infrared image sequences. In: *CNRS-ENSAM*, Bordeaux (France), 7–11 July 2014.
15. Previtali M, Barazzetti L, Redaelli V, Scaioni M and Rosina E. Rigorous procedure for mapping thermal infrared images on three-dimensional models of building façades. *J Appl Remot Sens* 2013; 7: 073503–073503.
16. Borenstein J, Everett H and Feng L. *Where am I? Sensors and methods for mobile robot positioning: Vol. 119*. Michigan, Ann Arbor: University of Michigan, 1996, p.27.
17. Riveiro B, Morer P, Arias P and De Arteaga I. Terrestrial laser scanning and limit analysis of masonry arch bridges. *Constr Build Mater* 2011; 25: 1726–1735.
18. Puente I, González-Jorge H, Martínez-Sánchez J and Arias P. Review of mobile mapping and surveying technologies. *Measurement* 2013; 46: 2127–2145.
19. Lagüela S, González-Jorge H, Armesto J and Herráez J. High performance grid for the metric calibration of thermographic cameras. *Meas Sci Technol* 2012; 23: 015402.
20. Taylor T, Counsell J and Gill S. Combining thermography and computer simulation to identify and assess insulation defects in the construction of building façades. *Energ Build* 2014; 76: 130–142.
21. ISO 6781:1983. *Thermal insulation, qualitative detection of thermal irregularities in building envelopes, infrared method*. Geneva: International Organization for Standardization, 1983.
22. Shih T and Faig W. A solution for space resection in closed form. *Int Arch Photogramm Remot Sens* 1988; 27: 547–56.
23. Ministerio de Fomento. Código Técnico de la Edificación, http://www.codigotecnico.org/images/stories/pdf/ahorroEnergia/DA-DB-HE-1-Calculo_de_parametros_caracteristicos.pdf (accessed 15 February 2016).
24. Pierrot-Deseilligny M, De Luca L and Remondino F. Automated image-based procedures for accurate artifacts 3D modeling and orthoimage generation. *Geoinform FCE CTU J* 2011; 6: 291–299.
25. Barrios G, Huelsz G, Rojas J, Ochoa JM and Marincic I. Envelope wall/roof thermal performance parameters for non air-conditioned buildings. *Energ Build* 2012; 50: 120–127.
26. Ministerio de Fomento. CTE. Syllabus of construction solution, http://cte-web.iccl.es/materiales.php (accessed 18 February 2014).
27. Liu L and Stamos I. Automatic 3D to 2D registration for the photorealistic rendering of urban scenes. In: *Proceedings of the 2005 IEEE computer society conference on computer vision and pattern recognition*, IEEE, San Diego, CA, December 2005; Vol. 2: pp.137–143.
28. Asdrubali F, Baldinelli G and Bianchi F. A quantitative methodology to evaluate thermal bridges in buildings. *Appl Energ* 2012; 97: 365–373.
29. González-Aguilera D, Rodriguez-Gonzalvez P, Armesto J and Lagüela S. Novel approach to 3D thermography and energy efficiency evaluation. *Energ Build* 2012; 54: 436–443.